

Article

# Enhanced Organic Pollutant Removal Efficiency of Electrospun NiTiO<sub>3</sub>/TiO<sub>2</sub>-Decorated Carbon Nanofibers

Ibrahim M. Maafa \*  and Mohammad Ashraf Ali 

Department of Chemical Engineering, College of Engineering, Jazan University, Jazan 45142, Saudi Arabia

\* Correspondence: imoafa@jazanu.edu.sa

**Abstract:** A nanocomposite comprised of nickel titanate/titania nanoparticles decorated with carbon nanofibers (NiTiO<sub>3</sub>/TiO<sub>2</sub>-decorated CNFs) is successfully synthesized via electrospinning and further utilized for methylene blue (MB) photodegradation. The morphology, phase, structural and chemical composition of the nanocomposite is investigated via scanning electron microscope, X-ray diffraction and transmission electron microscope equipped with energy dispersive X-ray. A mathematical model is developed to predict the photocatalytic activity of the produced nanocomposite by considering parameters such as initial dye concentration, light intensity, reaction temperature, and catalyst dosage. The reaction rate constant  $K_1$  decreased from 0.0153 to 0.0044 min<sup>-1</sup> with an increase in the MB concentration from 5 to 15 mg L<sup>-1</sup>, while  $K_2$ ,  $K_3$ , and  $K_4$  were found to increase with the increase in reaction temperature (0.0153 to 0.0222 min<sup>-1</sup>), light intensity (0.0153 to 0.0228 min<sup>-1</sup>) and catalyst dose concentration (0.0153 to 0.0324 min<sup>-1</sup>), respectively. The results obtained are found to be in good agreement with the modeling results and showed effective photodegradation activity. The performance of our catalyst is found to be better compared to other catalysts previously reported in the literature. The recyclability data of the synthesized NiTiO<sub>3</sub>/TiO<sub>2</sub>-decorated CNFs catalyst for four runs show that the catalyst is quite stable and recyclable. This nanocomposite photocatalyst offers a low-cost solution for wastewater pollution problems and opens new avenues to further explore the electrospinning method for the synthesis of nanocomposites.



**Citation:** Maafa, I.M.; Ali, M.A. Enhanced Organic Pollutant Removal Efficiency of Electrospun NiTiO<sub>3</sub>/TiO<sub>2</sub>-Decorated Carbon Nanofibers. *Polymers* **2023**, *15*, 109. <https://doi.org/10.3390/polym15010109>

Academic Editors: Irene S. Fahim, Ahmed K. Badawi and Hossam E. Emam

Received: 6 November 2022

Revised: 12 December 2022

Accepted: 16 December 2022

Published: 27 December 2022



**Copyright:** © 2022 by the authors. Licensee MDPI, Basel, Switzerland. This article is an open access article distributed under the terms and conditions of the Creative Commons Attribution (CC BY) license (<https://creativecommons.org/licenses/by/4.0/>).

**Keywords:** electrospinning; nickel titanate; nanofibers; photodegradation; mathematical modeling

## 1. Introduction

Organic pollutants produced from industrial water pose a serious threat to our environment, which will eventually affect the health of humans and aquatic life [1–3]. Therefore, solving this problem calls for urgent attention to not only get rid of these pollutants but also to overcome the shortage of usable fresh water. According to the UNESCO World Water Assessment Program (2003), about 2 million tons of disposed water from industrial and agricultural sources is released every day [4]. Thus, recycling and reusing disposed water has become a necessity. However, an effective and safe method to obtain usable water requires a high cost. Traditional methods such as chemical coagulation, flocculation, and adsorption have been employed to overcome the aforementioned issue; however, these methods suffer a major drawback in the formation of a secondary pollutant, and thus require additional steps to remove this, incurring an additional cost [5–9]. The photocatalytic process utilizing semiconducting materials is considered as an eco-friendly and inexpensive method for the decomposition and mineralization of untreated pollutants resulting from industrial wastewater employing ultraviolet or visible light irradiation [10,11]. Several photocatalytic semiconductors are being used in the decomposition of organic and inorganic pollutants. Titanium dioxide (TiO<sub>2</sub>) is the most common semiconductor utilized in the photocatalytic processes such as dye-sensitized solar cells (DSSC), photodegradation of untreated pollutants, self-cleaning paint, and water splitting [12–14]. TiO<sub>2</sub> is a low-cost material which is chemically stable, environmentally compatible, and easily available.

However, due to wide gap between its conduction and valence band ( $E_g \sim 3.0$  eV for rutile and  $E_g \sim 3.2$  eV for anatase) and its low quantum yield, it absorbs light in the UV region only, which impedes its practical application in photocatalysis [15,16]. Moreover, the quick recombination of light-induced electron ( $e^-$ ) and hole ( $h^+$ ) pairs leads to a decrease in the formation of radicals. The addition of metallic or non-metallic oxide to  $TiO_2$  leads to the formation of a narrow band gap and suppresses the recombination of photo-induced  $e^-$  and  $h^+$ , thereby shifting the absorption towards the visible spectrum [17,18]. During the past years, perovskite-based titanate has been introduced as an efficient photocatalyst in the visible spectrum [19–21]. Moreover, there has been a considerable attention focused on the fabrication of heterojunction structures of perovskite-based titanate and  $TiO_2$  [19–22]. Among them, nickel titanate ( $NiTiO_3$ ,  $E_g \sim 2.18$  eV) has been introduced as a competent photocatalyst in the degradation of untreated pollutants due to its suitable band gap and ability to absorb sunlight radiation [23]. Huang et al. synthesized  $NiTiO_3/TiO_2$  nanotubes and employed them for  $H_2$  production via the water splitting technique [24]. The synthesized material demonstrated good photocatalytic activity, as 45 and 680  $\mu\text{mol g}^{-1} \text{h}^{-1}$  for pristine  $TiO_2$  nanotube and synthesized material, respectively. Integration of a photocatalyst and adsorption could improve the overall wastewater treatment process. A combination of both processes could enhance the degradation performance of organic pollutants as compared to the individual processes [4]. Activated carbon is the most common adsorbent material and has been applied to various composites as support and an absorbent for photocatalyst material including  $TiO_2/AC$  [25],  $ZnO/AC$  [26], and  $CeO_2/AC$  [27]. Due to their unique properties, nano-carbon materials such as carbon nanofibers (CNFs), carbon nanotubes (CNT), and graphene have gained extensive interest and are widely used in various applications [28,29]. Moradi et al. incorporated graphene oxide (GO) with  $FeTiO_3$  to reduce its band gap and showed an enhanced shift towards the visible spectrum [30]. They demonstrated that the visible light offers faster degradation compared to the UV light. The material was synthesized via an ultrasound-assisted method and showed enhanced photocatalytic activity towards phenolic compound degradation under sunlight after 240 min. Their study reported that the rate of phenol removal was increased to 44% with an increase in addition of GO to  $FeTiO_3$  from 1 to 3%. GO works as a good  $e^-$  receiver, which inhibits electron and hole recombination. Furthermore, GO improved phenol adsorption in  $GO/FeTiO_3$ , wherein phenol readily reacts with hydroxyl radicals and holes present on the surface. The previous studies also show the enhanced photocatalytic activity of CNFs towards pollutant adsorption from water due to small pores and high surface area formed during the electrospinning process and calcination [31]. Besides the enhancement of adsorption, CNFs have high electrical conductivity, which promotes the capture and transfer of photo-induced charges during the photosynthesis process [32,33]. This present work reports the synthesis of heterojunction  $NiTiO_3/TiO_2$ -decorated CNFs and their visible-light-driven MB degradation as a model dye. The photocatalyst was synthesized employing an electrospinning technique followed by calcination at 800 °C of the electrospun nanofiber mats composed of titanium (IV) isopropoxide, nickel acetate tetrahydrate and poly(vinylpyrrolidone).

## 2. Experimental

### 2.1. Materials

Titanium isopropoxide (TiIP, 97%, Sigma Aldrich, St. Louis, MO, USA), poly(vinylpyrrolidone) (PVP, Sigma Aldrich, St. Louis, MO, USA) and nickel acetate tetrahydrate ( $(Ni(CH_3COO)_2 \cdot 4H_2O)$ , 98%) were obtained from Sigma-Aldrich, St. Louis, MO, USA. Methylene blue (95.0%) was procured from LOBA Chemie, India, while ethanol and acetic acid were obtained from Scharlau, Spain.

### 2.2. Synthesis of $NiTiO_3/TiO_2$ -Decorated CNFs

$NiTiO_3/TiO_2$ -decorated CNFs were prepared via a sol-gel process, by adding 1.5 mL of titanium isopropoxide into 10 wt% solution of poly(vinylpyrrolidone) prepared

in advance by dissolving 1.0 g of PVP in 10 mL deionized water at room temperature for 2 h duration under agitation. The poly(vinylpyrrolidone) solution was prepared as mentioned in previous reports [34–39]. The mixture was stirred until a transparent yellow gel was obtained. Then, nickel acetate tetrahydrate was added to this gel and continuously stirred until a green transparent gel was obtained. The prepared gel was fed into the plastic syringe of the lab-scale electrospinning device (NaBond Technologies Co., Limited, Hi Tech Park, Nanshan Dist., Shenzhen, Guangdong, China). The positive electrode was connected to the metallic end of the plastic syringe while the negative electrode was attached to the aluminum foil wrapped around the rotating cylinder. The voltage and distance between the positive and negative electrode during the spinning process were maintained at 20 kV and 15 cm, respectively. The NF mats formed on the surface of the aluminum foil were detached and placed in a vacuum dryer at a temperature of 50 °C for 24 h to get rid of the solvents. This was then calcined at 800 °C for 5 h. This synthesized material was named NiTiO<sub>3</sub>/TiO<sub>2</sub>-decorated CNFs. The TiO<sub>2</sub>@CNFs were prepared using a similar procedure except that the nickel acetate tetrahydrate was not added during gel preparation.

### 2.3. Catalyst Characterization

The morphological study of the NiTiO<sub>3</sub>/TiO<sub>2</sub>-decorated CNFs was performed by employing a scanning electron microscope (SEM Model JSM-5900, Japan Electron Optics Laboratory (JEOL Ltd., Tokyo, Japan) equipped with energy dispersive X-ray spectroscopic analysis (EDX). The crystallinity of the NFs was studied using an X-ray diffractometer (XRD, Rigaku Co., Tokyo, Japan) with Cu K $\alpha$  radiation ( $\lambda = 1.54056 \text{ \AA}$ ) in the range of 10° to 80° of two theta angles. A high-resolution transmission electron microscope (HRTEM) image was captured via JEOL Model JEM-2200FS, operated at 200 kV and equipped with EDX (JEOL Ltd., Tokyo, Japan).

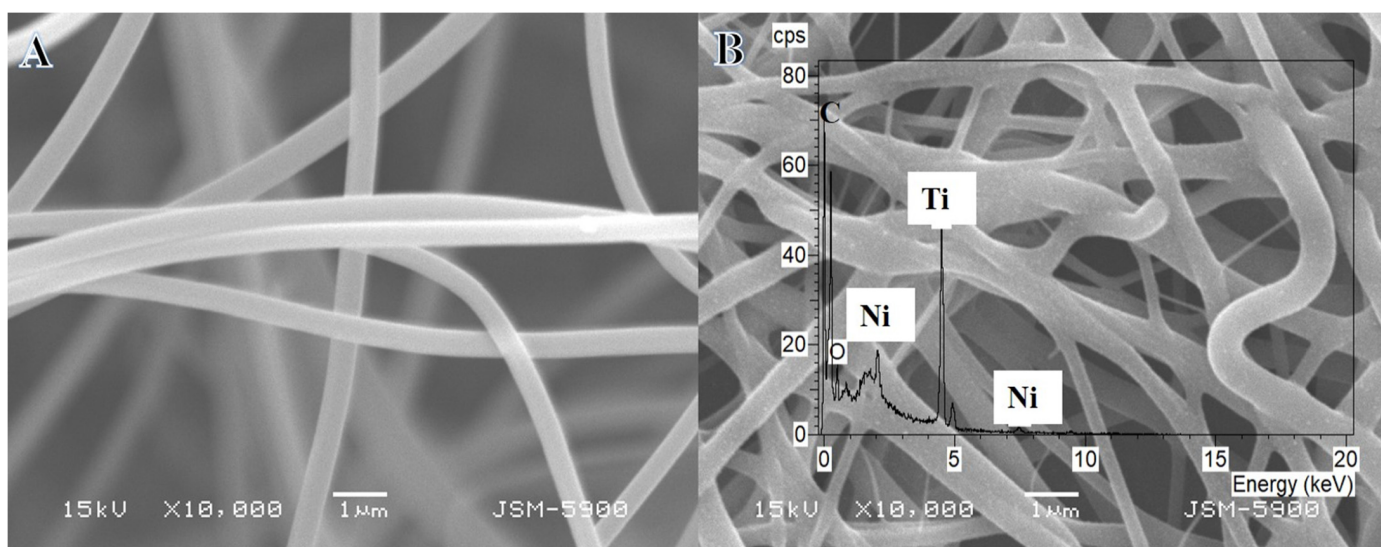
### 2.4. Determination of MB Photodegradation

The MB photo-degradation in the presence of NiTiO<sub>3</sub>/TiO<sub>2</sub>-decorated CNFs was carried out in a simple batch photo-reactor consisting of a simple laboratory borosilicate glass bottle (150 mL). A visible fluorescent lamp was used as the light source ( $\lambda = 420\text{--}700 \text{ nm}$ ,  $I = 23\text{--}40 \text{ Wm}^{-2}$  (Philips Co., Amsterdam, The Netherlands). The reactor (150 mL borosilicate glass bottle) was charged with 100 mL of MB aqueous solution with known concentration and a previously known amount of NiTiO<sub>3</sub>/TiO<sub>2</sub>-decorated CNFs photocatalyst. The solution was kept in the dark under continuous stirring for 20 min to determine the adsorption–desorption capacity of the photocatalyst towards MB. Later, the solution was stirred and exposed directly to the visible light radiation. The distance between the reactor and the lamp was 12 cm. The reaction temperature was controlled via a thermostat water bath. An aliquot of 3.0 mL of MB solution was withdrawn after specific time intervals under irradiation. The solution sample was centrifuged to separate the solid catalyst from the solution. Then, the filtered solution was introduced into a UV-visible spectrophotometer to determine the MB concentration present in the solution. The reaction parameters studied were MB concentration, reaction temperature, light intensity and the catalyst concentration.

## 3. Results and Discussion

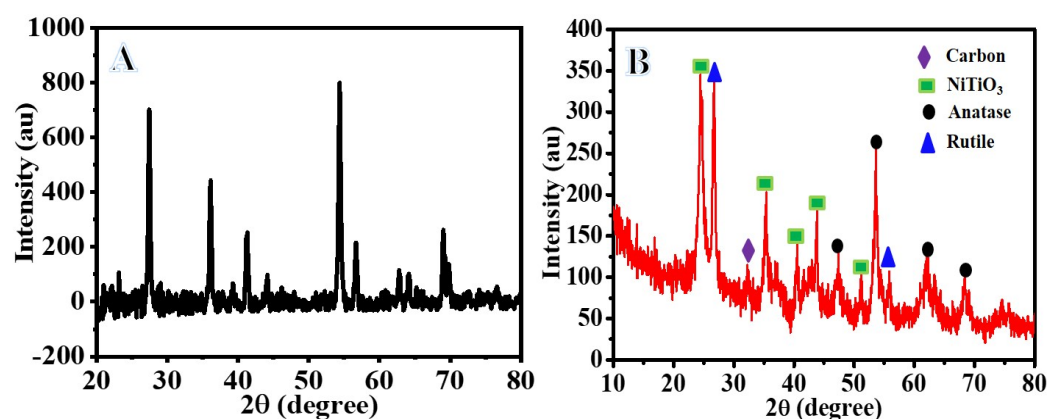
### 3.1. Catalyst Characterization

Figure 1A displays the SEM image of the electrospun nanofiber mat consisting of nickel acetate tetrahydrate, titanium isopropoxide, and poly(vinylpyrrolidone) after vacuum drying at 50 °C for 24 h. The image shows smooth and bead-free NFs. During the calcination process performed at 800 °C, NFs preserved their structure with the growth of tiny white NPs on the surface of NFs (Figure 1B). EDX analysis (Inset Figure 1B) indicates that the NFs mainly consisted of nickel (Ni), titanium (Ti), oxygen (O), and carbon (C), with the absence of any other element.



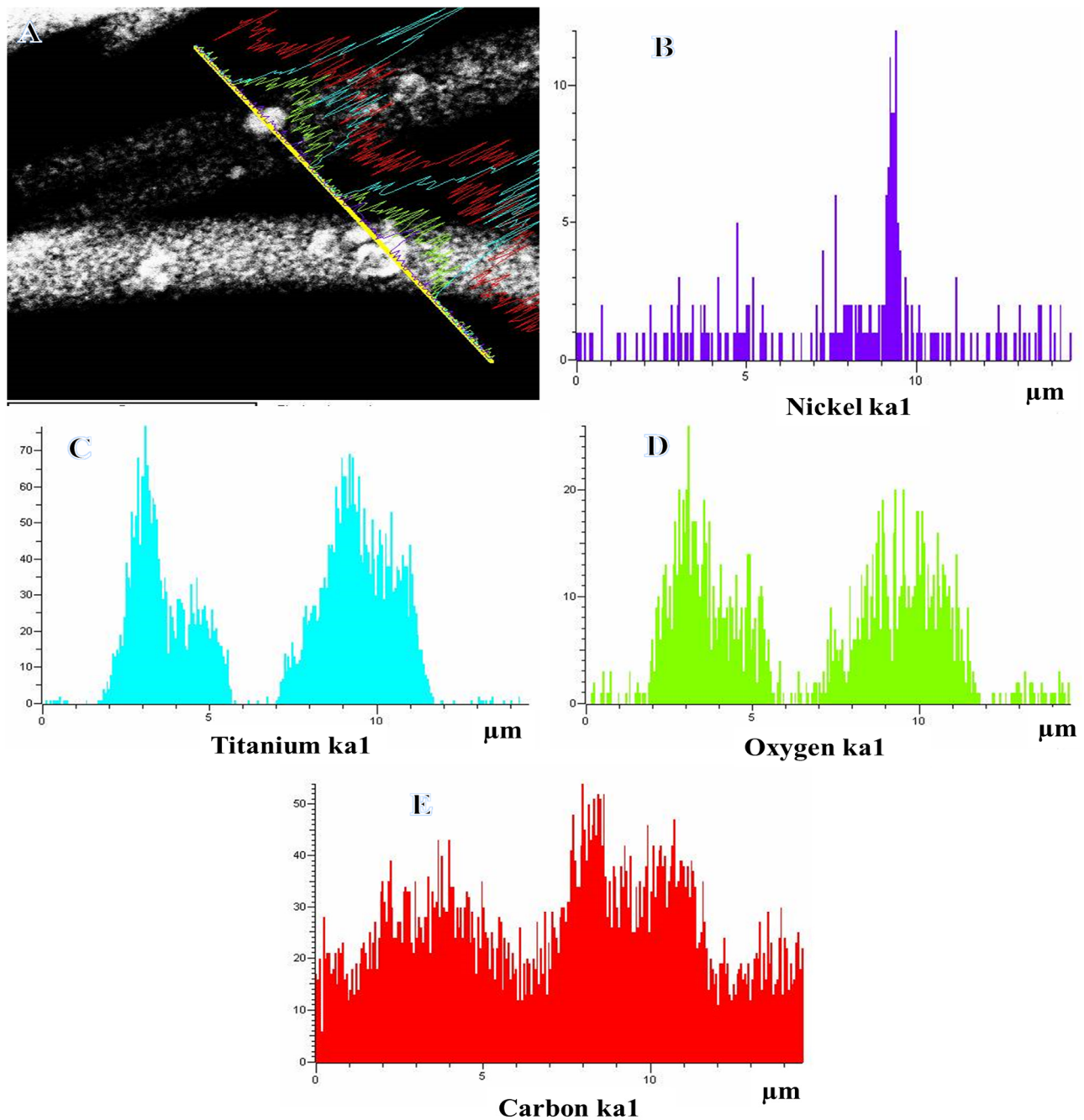
**Figure 1.** SEM images of the electrospun NiAc/TiIP/PVP nanofiber mats after drying at 50 °C overnight (A) and the produced NiTiO<sub>3</sub>/TiO<sub>2</sub>-decorated CNFs after calcination in argon at 800 °C (B).

Figure 2 displays the XRD patterns of the powder obtained after the calcination process. The results show the formation of TiO<sub>2</sub> phases at  $2\theta$  of 27.02° which corresponds to (110) crystal plane; rutile phase (JCPDS # 00-004- 0551) at  $2\theta$  of 47.5°, 53.7°, 62.1°, 68.4° which agree with the (200), (105), (204), (220) plane, respectively; anatase phase (JCPDS # 21-1272). In addition, there is a formation of a hexagonal ilmenite NiTiO<sub>3</sub> phase (JCPDS#01-039-12035) at  $2\theta$  of 24.4°, 35.5°, 40.6°, 43.7°, 50.9°, which match with (012), (110), (113), (202), (107), and (211) crystal planes, respectively. The low intensity peak observed at  $2\theta$  value of 32.4° is in agreement with the (002) plane of carbon-like graphite, which is formed due to the partial decomposition of carbon during the calcination process.



**Figure 2.** XRD patterns of the produced powder after calcination of electrospun TiIP/PVP (A) and NiAc/TiIP/PVP (B) nanofiber mats at 800 °C in argon atmosphere.

TEM EDX was performed to determine the chemical composition of synthesized NFs (Figure 3). Figure 3A displays the TEM image of a single selected NF along with the line TEM-EDX analysis and the corresponding EDX analysis is displayed in Figure 3B–E. It is evident from the figure that Ti, O, Ni, and C have the same distribution, which confirmed the formation of the NiTiO<sub>3</sub>-TiO<sub>2</sub> composite. The carbon was covered with NiTiO<sub>3</sub>-TiO<sub>2</sub> composite (Figure 3A). The presence of carbon may be enhancing the overall photocatalytic process through the enhanced photo-induced e<sup>-</sup> and h<sup>+</sup> separation, the more exposed area to the pollutant and the enhanced photodegradation rate.



**Figure 3.** TEM image for a single calcined nanofiber along with the line TEM EDX analysis (A) and the corresponding Ti, C, O and Ni line analyses TEM EDX (B–E).

### 3.2. Photocatalytic Degradation of MB

To understand the photodegradation process of MB dye using NiTiO<sub>3</sub>/TiO<sub>2</sub>-decorated CNFs catalyst, we considered the effect of MB dye concentration ( $C_i$ ), reaction temperature ( $T$ ), photocatalyst dosage (NiTiO<sub>3</sub>/TiO<sub>2</sub>-decorated CNFs), and light intensity ( $I$ ). The following mathematical model is designed to predict the photocatalytic reaction as a function of the studied parameters [40]:

$$K_{app} = K' \left( \frac{K_R}{1 + K_R C_i} \right) \left( \exp \frac{-E_a}{RT} \right) (mI) \left( \frac{K_{NFs} C_{NFs}}{1 + K_{NFs} C_{NFs}} \right) \quad (1)$$

Figure 4 shows the change of MB concentration versus irradiation time in the absence of photocatalytic NFs, and in the presence of  $\text{TiO}_2$ @CNFs and  $\text{NiTiO}_3/\text{TiO}_2$ @CNFs. It can be observed from Figure 4 that the efficiency of MB photodegradation using  $\text{NiTiO}_3/\text{TiO}_2$ -decorated CNFs is higher than that of  $\text{TiO}_2$ @CNFs. After 120 min of visible light irradiation, enhanced photodegradation of 82.4% and 62.5% is achieved for  $\text{NiTiO}_3/\text{TiO}_2$ -decorated CNFs and  $\text{TiO}_2$ @CNFs, respectively. This achievement of 20% increase in photodegradation activity is significant.  $\text{TiO}_2$  alone is not very active under visible irradiation, however when  $\text{TiO}_2$  is doped with carbon, the band gap of titania narrows which makes it active under visible irradiation [3].

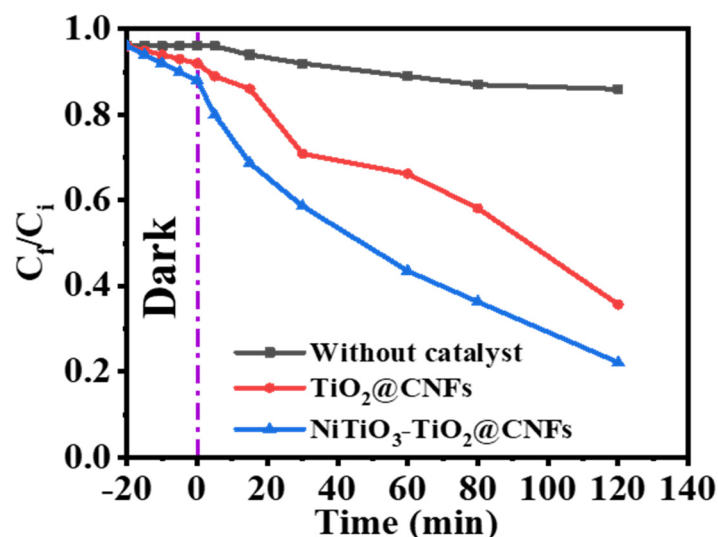


**Figure 4.** The photodegradation profile of MB dye. The parameters are: photocatalyst amount =  $0.2 \text{ gm L}^{-1}$ ,  $C_i = 0.1 \text{ M}$ ,  $T = 298 \text{ K}$ , and  $I = 25 \text{ W m}^{-2}$ .

### 3.2.1. Effect of Initial Dye Concentration ( $C_i$ )

We studied the effect of initial MB dye concentration (5, 7.5, 10, and  $15 \text{ mg L}^{-1}$ ) on the photodegradation reaction under visible light irradiation in the presence of  $\text{NiTiO}_3/\text{TiO}_2$ -decorated CNFs. As seen in Figure 5A, the MB photodegradation decreases with increasing MB concentration, which may be plausibly due to the limited production of active radicals in the photocatalytic process at higher MB concentrations [30,41]. Furthermore, higher concentration of MB dye could absorb more light and cause the prevention of photons to reach to the surface of the photocatalyst, thereby reducing the efficiency of the photodegradation process [42–44]. Thus, the photodegradation process is efficient at low concentrations because of more available active sites on the surface of the photocatalyst to adsorb dye molecules. Photodegradation of organic compounds can be described through a pseudo-first order reaction according to the Langmuir Hinshelwood (LH) model (Equation (2)).

$$r_{\text{MB}} = -\frac{dC_f}{dt} = K_1 C_f \quad (2)$$

$$r_{\text{MB}} = \frac{K_{\text{LH}} K_{\text{R}} C_f}{1 + K_{\text{R}} C_i} \quad (3)$$

$$r_{\text{MB}} = \frac{K_{\text{LH}} K_{\text{R}} C_f}{1 + K_{\text{R}} C_i} = K_1 C_f \quad (4)$$

$$K_1 = \frac{K_{\text{LH}} K_{\text{R}}}{1 + K_{\text{R}} C_i} \quad (5)$$

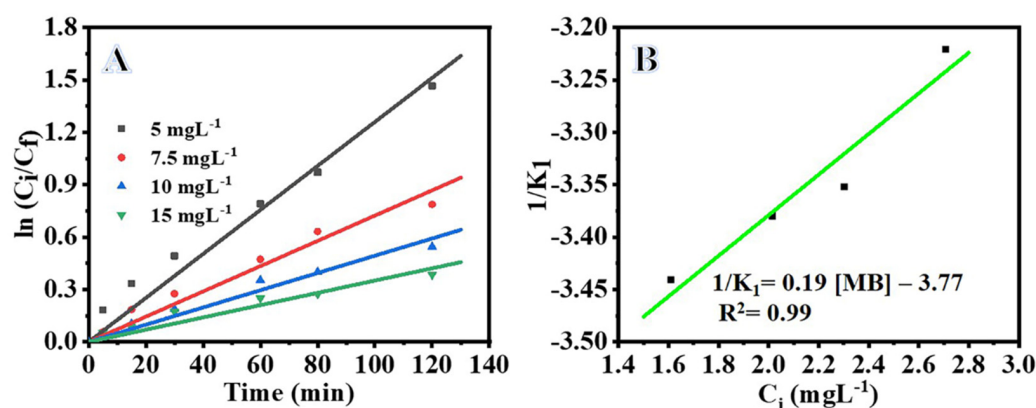


**Figure 5.** Influence of [MB] on photodegradation of MB, (A)  $\ln C_i/C_f$  vs. time (B) modified LH plot for MB photodegradation. The parameters are: photocatalyst amount =  $0.2 \text{ gm L}^{-1}$ ,  $C_i = 0.1 \text{ M}$ ,  $T = 298 \text{ K}$ , and  $I = 25 \text{ W m}^{-2}$ .

Figure 5A shows the kinetics of the MB degradation over the  $\text{NiTiO}_3/\text{TiO}_2$ -decorated CNFs at various concentrations. The value of rate constant ( $K_1$ ) can be determined from the slope of the straight line obtained in Figure 5B. The value of  $K_1$  decreases from  $0.0153$  to  $0.0044 \text{ min}^{-1}$  with the increase of MB concentration from  $5$  to  $15 \text{ mg L}^{-1}$  (Table 1), which may be plausibly due to the limited formation of active radicals at higher concentrations. The relationship between  $K_1$  and  $C_i$  is obtained via a  $1/K_1$  versus  $C_i$  plot (Figure 5B) and modified LH model by transforming Equation (6).

$$\frac{1}{K_1} = \frac{1}{K_{\text{LH}}}C_i + \frac{1}{K_{\text{LH}}K_{\text{R}}} \quad (6)$$

to a straight-line equation  $y = ax + b$ , where

$$x = C_i$$

$$a = 1/K_{\text{LH}}$$

$$K_{\text{LH}} = 1/a = 1/17.595 = 5.683 \times 10^{-2}$$

$$b = 1/(K_{\text{LH}}K_{\text{R}})$$

$$K_{\text{R}} = 1/(K_{\text{LH}} \times b) = 1/(5.683 \times 10^{-2} \times 4.7345) = 3.378$$

**Table 1.** Rate constants of reactions of MB photodegradation at various MB concentrations, reaction temperatures, light intensities, and  $\text{NiTiO}_3/\text{TiO}_2$ -decorated CNFs catalyst doses.

MB Dye Concentration ( $\text{mg L}^{-1}$ )	Rate Constant ( $\text{min}^{-1}$ ) $K_1$
5	0.0153
7.5	0.0088
10	0.0068
15	0.0044
Reaction temperature ( $^{\circ}\text{C}$ )	Rate constant ( $\text{min}^{-1}$ ) $K_2$
25	0.0153
30	0.0166
35	0.0188
40	0.0222
Light intensity ( $\text{W/m}^2$ )	Rate constant ( $\text{min}^{-1}$ ) $K_3$
25	0.0153
30	0.0166
35	0.019
40	0.0228
Catalyst dose ( $\text{mg L}^{-1}$ )	Rate constant ( $\text{min}^{-1}$ ) $K_4$
200	0.0153
400	0.0216
600	0.027
800	0.0324

### 3.2.2. Effect of Reaction Temperature (T)

Figure 6A depicts the variation of photodegradation of MB versus irradiation time at various reaction temperatures. As shown in the figure, the photodegradation of MB increased with the increase in reaction temperature from 25 to 40 °C due to improved charge transfer at higher temperatures. The movement of electron–hole pairs becomes more active as the reaction temperature increases, which leads to the reaction between electrons, adsorbed oxygen and holes, and faster generation of hydroxyl radicals and hydroxyl ions, consequently improving the photodegradation of MB dye [45–47]. The temperature range of 20–80 °C is considered best for the effective photodegradation of organic compounds [45,48]. Further increases in the temperature could reduce the photocatalytic activity since the electron–hole recombination rate increased [45]. At the same time, low reaction temperature leads to reduction in the solubility of MB in water, causing partial condensation of MB in water [45,49].

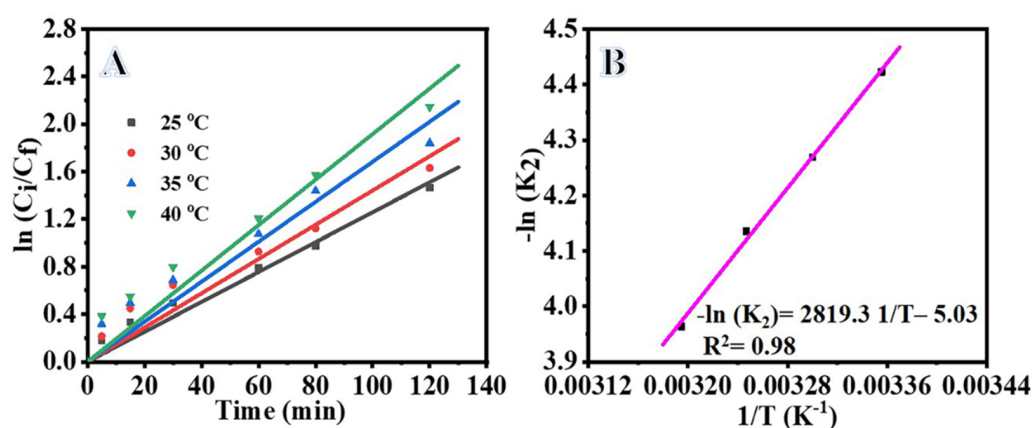


**Figure 6.** Influence of reaction temperature on photodegradation of MB (A),  $\ln C_i/C_f$  vs. time (B), Arrhenius plot for MB photodegradation. The parameters are: photocatalyst amount = 0.2 gm  $L^{-1}$ ,  $C_i = 0.1$  M, and  $I = 25$  W  $m^{-2}$ .

Figure 6B shows the kinetic study of MB photodegradation over the  $NiTiO_3/TiO_2$ -decorated CNFs at various temperatures. The value of reaction rate ( $K_2$ ) increased from 0.0153 to 0.0222  $min^{-1}$  with the increase of reaction temperature from 25 to 40 °C (Table 1), indicating an enhancement in the MB photodegradation efficiency with increasing temperature due to higher charge mobility. The rate constant ( $K_2$ ) can be determined from the slope of the straight line obtained in Figure 6B. The plot of  $K_2$  versus  $1/T$  gives a straight-line relationship. We apply the Arrhenius equation Equation (7) to obtain the activation energy ( $E_a$ ) of the photocatalytic reaction.

$$K_2 = A \exp \frac{E_a}{RT} \quad (7)$$

Applying the natural log (Ln) to both sides of Equation (7) removes the exponent to obtain Equation (8) as follows:

$$\ln K_2 = \left( \frac{E_a}{R} \right) \left( \frac{1}{T} \right) + \ln A \quad (8)$$

Transforming Equation (8) to a straight-line equation,  $y = ax + b$ , where

$$x = 1/T$$

$$a = E_a/R$$

$$E_a = a \times R = 2819.3 \times 8.314 = 2.344 \times 10^4$$

### 3.2.3. Effect of Light Intensity (I)

The photodegradation rate of organic compounds is affected by the light intensity and wavelength [42,50–52]. Figure 7A shows the influence of light intensity on the MB photodegradation. It is evident from the figure that the rate of MB photodegradation increased with the increase in light intensity. An increase in light intensity means the availability of a large number of photons, which improved the MB photodegradation. The rate constant ( $K_3$ ) can be determined from the slope of straight lines obtained from the plot of  $\ln(C_i/C_f)$  versus time at various light intensities (Figure 7A). The value of  $K_3$  increased from 0.0153 to 0.0228  $\text{min}^{-1}$  with the increase in light intensities from 25 to 40  $\text{Wm}^{-2}$  (Table 1), which indicates an enhancement in the MB photodegradation with increasing light intensity. The correlation between  $K_3$  and I is obtained by plotting  $1/K_1$  versus I (Figure 7B) and applying Equation (9) [40], since  $K_3$  is directly proportional to I as demonstrated in the following relationship:

$$K_3 = mI \quad (9)$$

Transforming Equation (9) to a straight-line equation,  $y = ax + b$ , where

$$x = I$$

$$a = m$$

$$m = 5 \times 10^{-4}$$

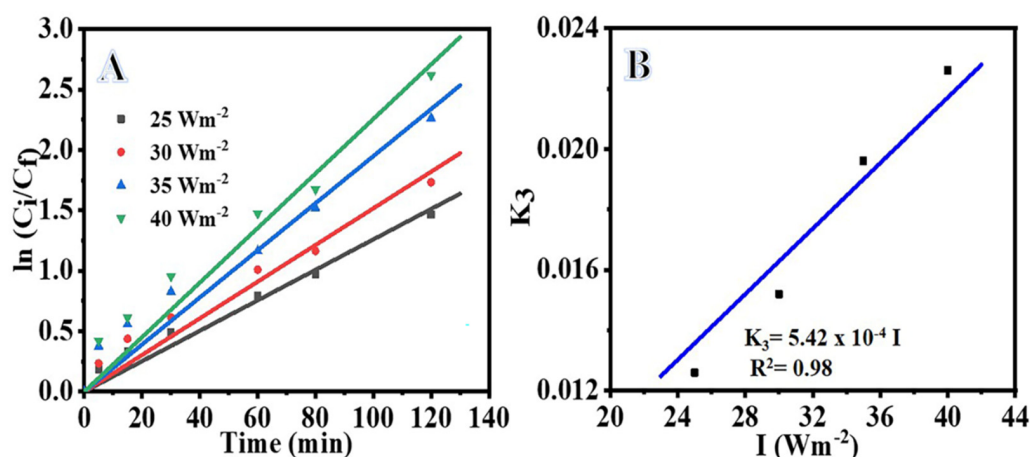


**Figure 7.** Influence of light intensity on photodegradation of MB, (A)  $\ln C_i/C_f$  vs. time (B) plot of  $K_3$  vs. I. The parameters are: photocatalyst amount = 0.2  $\text{gm L}^{-1}$ ,  $C_i = 0.1 \text{ M}$  and  $T = 298 \text{ K}$ .

### 3.2.4. Effect of Photocatalyst Dose ( $\text{NiTiO}_3/\text{TiO}_2$ -Decorated CNFs)

Figure 8A shows the variation of MB concentration versus irradiation time at various  $\text{NiTiO}_3/\text{TiO}_2$ -decorated CNFs doses (200, 300, 400, and 500  $\text{mg L}^{-1}$ ). As evident from the figure, the MB photodegradation increases with the increase in  $\text{NiTiO}_3/\text{TiO}_2$ -decorated CNFs dose, which may be plausibly due to increases in the available surface area of the  $\text{NiTiO}_3/\text{TiO}_2$ -decorated CNFs that improved the MB photodegradation. Furthermore, it is observed that the MB photodegradation at 400  $\text{mg L}^{-1}$  is very close to the dose at 500  $\text{mg L}^{-1}$ . This could be plausibly due to decreases in the active sites resulting from the aggregation phenomenon at high doses of  $\text{NiTiO}_3/\text{TiO}_2$ -decorated CNFs. This also causes light scattering and screening effects that decrease the photoreactions and active radicals [30,53–55]. Figure 8B shows the kinetic study of MB photodegradation over  $\text{NiTiO}_3/\text{TiO}_2$ -decorated CNFs at various catalyst doses. The value of reaction rate ( $K_4$ ) increases from 0.0153 to 0.0324  $\text{min}^{-1}$  with the increase in the photocatalyst dose from 200 to 500  $\text{mg L}^{-1}$  (Table 1), indicating an improvement in the MB photodegradation because an increased  $\text{NiTiO}_3/\text{TiO}_2$ -decorated CNFs dose provides comparatively high

active catalytic sites on the surface. The influence of NiTiO<sub>3</sub>/TiO<sub>2</sub>-decorated CNFs dosage on K<sub>4</sub> is determined by employing a Langmuir-type relationship, Equation (10) [40,56]:

$$K_4 = \frac{K_0 K_{NFs} C_{NFs}}{1 + K_{NFs} C_{NFs}} \quad (10)$$

This equation can be transformed to a straight-line equation, Equation (11), as follows:

$$\frac{1}{K_4} = \frac{1}{K_0 K_{NFs}} \left( \frac{1}{C_{NFs}} \right) + \frac{1}{K_0} \quad (11)$$

The straight-line equation is  $y = ax + b$ , where

$$x = 1/C_{NFs}$$

$$b = 1/K_0$$

$$K_0 = 1/3.042 = 0.3287$$

$$a = 1/K_0 K_{NFs}$$

$$K_{NFs} = 1/(17055 \times 0.3287) = 1.783 \times 10^{-4}$$

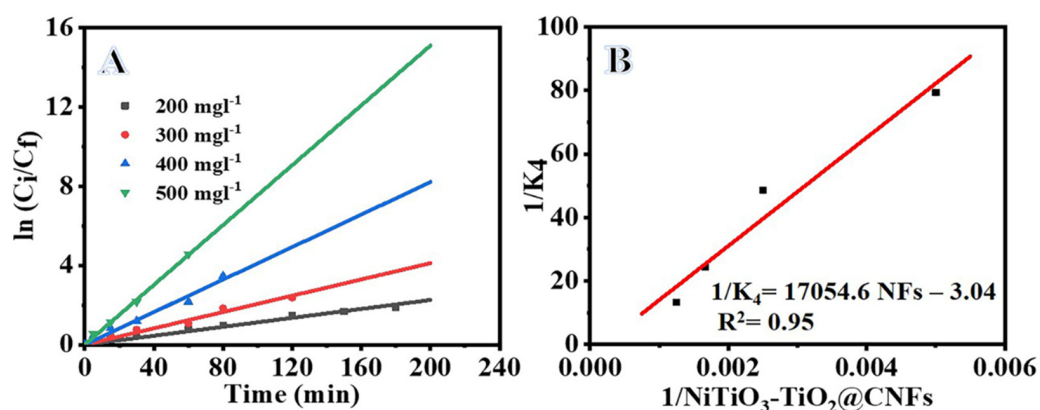


**Figure 8.** Influence of catalyst amount on photodegradation of MB (A),  $\ln C_i/C_f$  vs. time (B), Langmuir-type plot for photodegradation of MB. Parameters are:  $C_i = 0.1$  M,  $T = 298$  K, and  $I = 25$  W m<sup>-2</sup>.

Figure 9 shows the low- and high-magnification SEM images after using 500 mg L<sup>-1</sup> catalyst dosage. As seen in the figure, the photocatalyst kept the nanofibrous structure intact after the photodegradation process. This shows the stability of the nanofibrous catalyst.

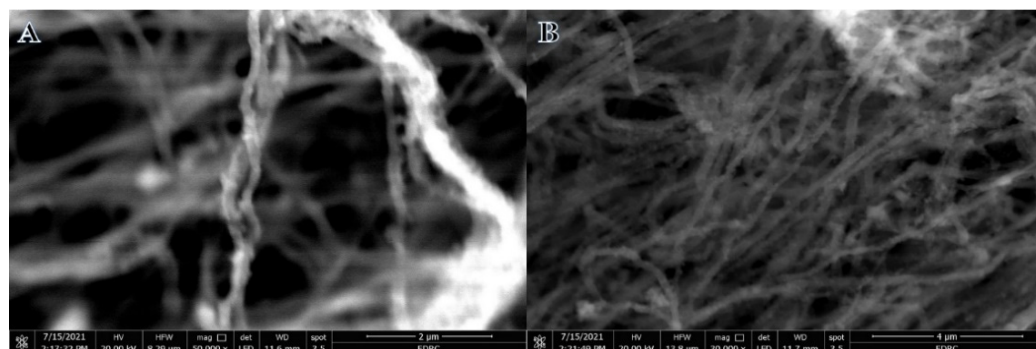


**Figure 9.** SEM images of the used photocatalyst. (A) 50,000 magnification, (B) 30,000 magnification.

### 3.2.5. Development of Model Rate Equation

The aforementioned results indicate that the rate constant is a function of MB concentration, reaction temperature, light intensity, and NiTiO<sub>3</sub>/TiO<sub>2</sub>-decorated CNFs dose according to Equations (6), (8), (9) and (11). The determined values of  $K_R$ ,  $E_a$ ,  $m$ , and  $K_{cat}$  employing multiple regression analysis are shown in Table 2. The equation constant  $k'$

is calculated using Equation (2) by substituting the previously obtained values of  $C_i$ ,  $T$ ,  $I$ ,  $C_{TiO_2}$  and values from Table 2.  $K_{app}$  can be rewritten as follows:

$$K_{app} = K' \left( \frac{3.378}{1 + 3.378 \times 5} \right) \left( \exp \frac{-2.344 \times 10^4}{8.314 \times 298} \right) (5 \times 10^{-4} \times 25) \left( \frac{1.78 \times 10^{-4} \times 200}{1 - 1.78 \times 10^{-4} \times 200} \right) \quad (12)$$

**Table 2.** Constant values obtained using multiple regression analysis for model equation.

Parameter	$k'$	$K_R$ (L mg <sup>-1</sup> )	$E_a$ (J mol <sup>-1</sup> )	$R$ (J K <sup>-1</sup> mol <sup>-1</sup> )	$m$ (m <sup>2</sup> W <sup>-1</sup> min <sup>-1</sup> )	$K_{NFs}$ (L mg <sup>-1</sup> )
Values	$3.7551 \times 10^4$	4.99	$1.9204 \times 10^4$	8.314	$6 \times 10^{-4}$	$2.444 \times 10^{-3}$

From Figure 2,  $K_{app}$  = reaction rate constant = 0.0153.

$$0.0126 = K' \left( \frac{3.378}{1 + 3.378 C_i} \right) \left( \exp \frac{-2.344 \times 10^4}{8.314 T} \right) (5 \times 10^{-4} I) \left( \frac{-1.78 \times 10^{-4} C_{CNF}}{1 - 1.78 \times 10^{-4} C_{CNF}} \right)$$

$$K' = -1.857908 \times 10^6$$

$$K_{app} = -1.857908 \times 10^6 \left( \frac{3.378}{1 + 3.378 C_i} \right) \left( \exp \frac{-2.344 \times 10^4}{8.314 T} \right) (5 \times 10^{-4} I) \left( \frac{-1.78 \times 10^{-4} C_{CNF}}{1 - 1.78 \times 10^{-4} C_{CNF}} \right)$$

A comparison between the experimental data and the determined  $K_{app}$  for the MB photodegradation at various conditions is shown in Figure 10. The obtained plot shows that the experimental data are in good agreement with the model-calculated data, which confirms the authenticity of our model to predict the reaction rate constant at various operational conditions.

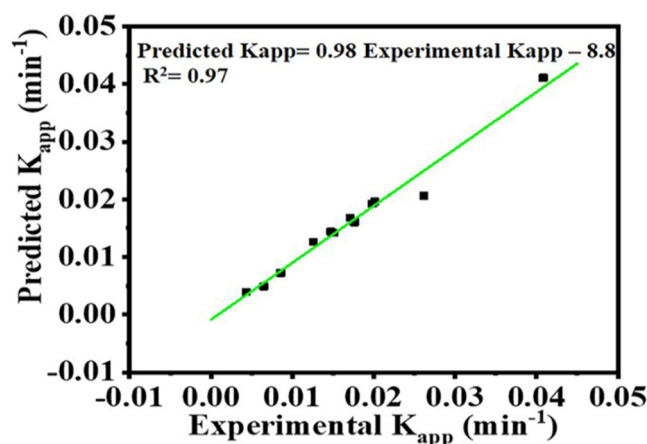


**Figure 10.** Comparison of experimental  $K_{app}$  and predicted  $K_{app}$  values.

### 3.3. Photocatalytic Mechanism

The photocatalytic mechanism is proposed for the NiTiO<sub>3</sub>/TiO<sub>2</sub>-decorated CNFs in the photodegradation of MB dye. The band alignment and charge transfer diagram of the NiTiO<sub>3</sub>/TiO<sub>2</sub>-decorated CNFs is shown in Figure 11. The photocatalytic process is responsible for the production of active radicals and ions. However, the higher bandgap of TiO<sub>2</sub> is responsible for the production of fewer active radicals in visible light [57].

The separation of the photogenerated electron–hole pairs across the NiTiO<sub>3</sub>/TiO<sub>2</sub>-decorated CNFs may be ascertained by calculating the conduction band (CB) and valence band (VB) potentials of the components. Specifically, these energies are calculated using the following empirical formulae:

$$E_{CB} = \chi - E^e - 0.5E_g \quad (13)$$

$$E_{VB} = E_{CB} + E_g \quad (14)$$

where the VB potential is denoted by  $E_{VB}$ , and the CB potential is denoted by  $E_{CB}$ .  $E^e$  is the energy of free electrons versus NHE, which is 4.5 eV [57,58].  $E_g$  is the band gap energy of the semiconductor. Finally, the electronegativity of the semiconductor is denoted by the letter  $\chi$ .

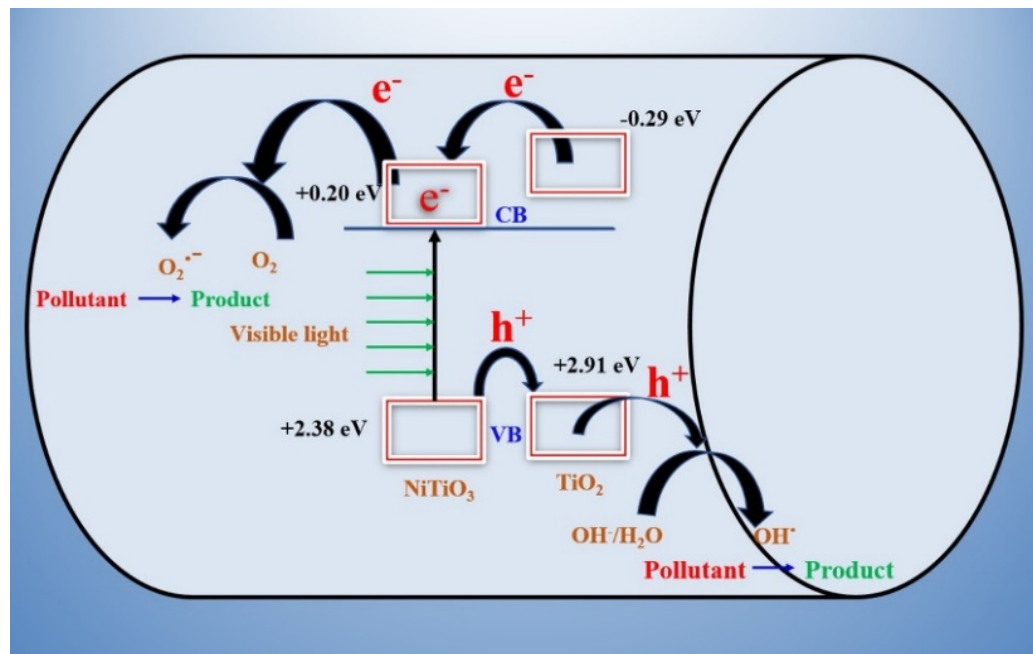
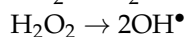
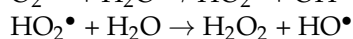
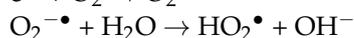
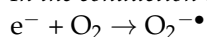


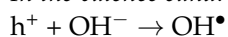
**Figure 11.** Schematic diagram for the creation and influence of electrons and holes in the photocatalytic degradation of MB.

The conduction band (CB) and valence band (VB) potentials of NiTiO<sub>3</sub> with respect to the standard hydrogen electrode (SHE) are 0.23 eV and +2.62 eV, respectively [58]. The NiTiO<sub>3</sub> has smaller bandgap (2.62 eV) than pure TiO<sub>2</sub> (3.2 eV), thus the VB position of NiTiO<sub>3</sub> is higher than TiO<sub>2</sub> (+2.7 eV), which enables the hole transfer from the VB of NiTiO<sub>3</sub> to the VB of TiO<sub>2</sub>. The resulting photogenerated hole ( $h^+$ ) reacts with H<sub>2</sub>O/OH<sup>-</sup> to produce hydroxyl radicals [30,59], while CB of NiTiO<sub>3</sub> is located at a lower position than that of TiO<sub>2</sub>. As light irradiates, the electrons in the VB of NiTiO<sub>3</sub> get excited and reach CB, which results in partial vacancy in the VB, and the electrons from the CB of TiO<sub>2</sub> get transferred to the CB of NiTiO<sub>3</sub>. The role of NiTiO<sub>3</sub> in the photocatalytic mechanism suggests that it can be used as an efficient sensitizer under visible light. The photogenerated electrons in NiTiO<sub>3</sub> move freely towards the surface of the CNFs, suggesting the low recombination of photogenerated electrons and holes [60]. The oxygen molecules react with the photogenerated electrons in the CB of NiTiO<sub>3</sub> to produce  $\bullet O_2^{-}$  without recombining with the holes present on the surface of TiO<sub>2</sub> [36]. The resulting  $\bullet O_2^{-}$  react with the hydrogen ion and produce HOO $\bullet$ , which consequently alter the MB molecule in the solution. The achieved photocatalytic activity of the NiTiO<sub>3</sub>/TiO<sub>2</sub> heterojunction is higher than that of the pure TiO<sub>2</sub> [61]. The photodegradation mechanism of MB using NiTiO<sub>3</sub>/TiO<sub>2</sub>-decorated CNFs can be explained as follows [1,30]:

*In the conduction band:*



*In the valence band:*



### 3.4. Catalyst Recyclability Data

The stability and recyclability of the synthesized NiTiO<sub>3</sub>/TiO<sub>2</sub>-decorated CNFs catalyst is tested for MB photodegradation. Figure 12 shows the catalyst recyclability data of the catalyst after 120 min of visible light irradiation for four consecutive runs. The photodegradation activity of the catalyst showed very little decrease (~1.3%) after four runs. The data show that the catalyst is stable and recyclable.

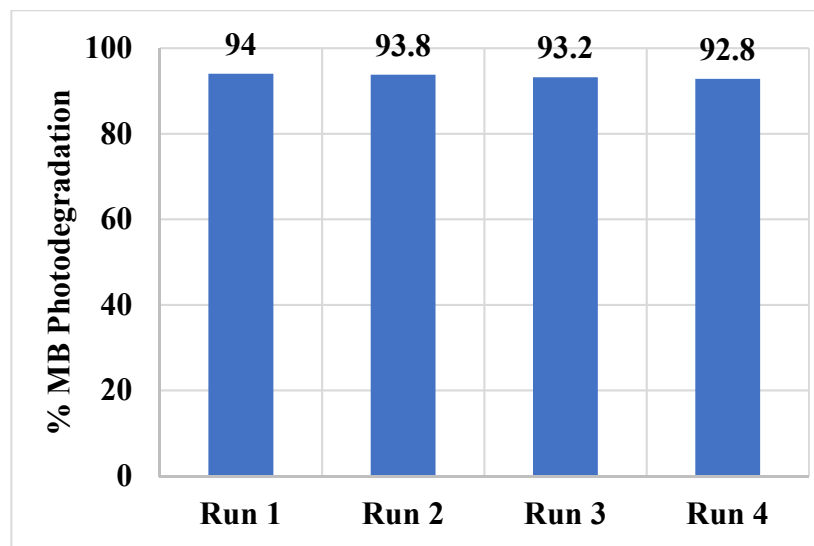


**Figure 12.** Catalyst recyclability data of NiTiO<sub>3</sub>/TiO<sub>2</sub>-decorated CNFs after 120 min of visible light irradiation.

### 3.5. Comparison of Our Results with the Literature

The results obtained from the photocatalytic degradation of MB in the presence of catalyst NiTiO<sub>3</sub>/TiO<sub>2</sub>-decorated CNFs is compared with the catalysts reported in the literature with titanate as an active ingredient. The results are reported in Table 3. Marco Alejandro Ruiz Preciado demonstrated the photocatalytic activity of NiTiO<sub>3</sub> for the photodegradation of MB using thin films under visible light [62]. Their study determined a reaction rate constant of 0.0030 min<sup>-1</sup>. Dao et al. synthesized co-doped NiTiO<sub>3</sub>/g-C<sub>3</sub>N<sub>4</sub> composite photocatalysts and used them for MB photodegradation under visible light irradiation [63]. The combination of co-doped NiTiO<sub>3</sub> and g-C<sub>3</sub>N<sub>4</sub> enhanced the photocatalytic performance of the composite photocatalyst. The co-doped composite photocatalyst (1% co-doped NiTiO<sub>3</sub>/g-C<sub>3</sub>N<sub>4</sub>) produced a higher  $k_{app}$  value (0.0072 min<sup>-1</sup>), while the one loaded with 3% co-doped NiTiO<sub>3</sub>/g-C<sub>3</sub>N<sub>4</sub> showed a lower value of the rate constant (0.0057 min<sup>-1</sup>). Kitchamsetti et al. synthesized MnTiO<sub>3</sub> perovskite nanodiscs and utilized them for the photocatalytic degradation of several organic dyes [64]. These nanodiscs provide stable and recyclable photocatalytic activity under Xenon lamp irradiation. The results showed 89.7, 80.4, 79.4, and 79.4% degradation of MB, rhodamine B, Congo red, and methyl orange at rate constants of 0.011, 0.006, 0.007, and 0.009 min<sup>-1</sup>, respectively. Sadjadi et al. reported the synthesis of NiTiO<sub>3</sub> NPs loaded on MCM-41 and used them for the photocatalytic degradation of MB under UV and visible light irradiation [65]. The results showed that the NiTiO<sub>3</sub> NPs/MCM-41 composite has higher photocatalytic activity than that of NiTiO<sub>3</sub> NPs and exhibited a kinetic rate constant of 0.018 min<sup>-1</sup>. Khan et al. synthesized one-dimensional NiTiO<sub>3</sub> NFs via electrospinning method and loaded them with acetic acid-treated, exfoliated and sintered sheets of graphitic carbon nitride (AAs-gC<sub>3</sub>N<sub>4</sub>), which produced a unique heterogeneous structure [66]. The weight ratio of NiTiO<sub>3</sub> NFs to porous AAs-gC<sub>3</sub>N<sub>4</sub> was 40:60, and displayed very good photodegradation of MB at a rate constant of 0.0310 min<sup>-1</sup>. This comparison clearly showed that the NiTiO<sub>3</sub>/TiO<sub>2</sub>-decorated CNFs catalyst possesses a high kinetic rate constant (0.0324 min<sup>-1</sup>) compared to other reported catalysts.

**Table 3.** Performance comparison of our catalyst with those reported in the literature.

Catalyst Used	Rate Constant ( $\text{min}^{-1}$ )	References
NiTiO <sub>3</sub> NFs	0.0030	[62]
1%Co-NiTiO <sub>3</sub> /g-C <sub>3</sub> N <sub>4</sub>	0.0072	[63]
3%Co-NiTiO <sub>3</sub> /g-C <sub>3</sub> N <sub>4</sub>	0.0057	[63]
MnTiO <sub>3</sub> perovskite nanodiscs	0.0110	[64]
NiTiO <sub>3</sub> NFs/MCM-41	0.0189	[65]
NiTiO <sub>3</sub> NFs/40wt% AAs-gC <sub>3</sub> N <sub>4</sub>	0.0310	[66]
NiTiO <sub>3</sub> /TiO <sub>2</sub> -decorated CNFs	0.0324	Our work

#### 4. Conclusions

Electrospinning and calcination methods are utilized in the successful synthesis of NiTiO<sub>3</sub>/TiO<sub>2</sub>-decorated CNFs. The chemical composition, structural information, and phase analysis are evaluated via characterization techniques which confirm the fabrication of CNFs. Several operational parameters for the photodegradation application, such as the effect of the initial dye concentration, reaction temperature, light intensity, and catalyst dose, are considered. A successful model is achieved through the determination of reaction rate constant ( $k_{app}$ ) to predict the photocatalytic activity of the composite NiTiO<sub>3</sub>/TiO<sub>2</sub>-decorated CNFs towards photodegradation of MB dye under visible light in a batch reactor. The photodegradation is 82.4% and 62.5% for NiTiO<sub>3</sub>/TiO<sub>2</sub>-decorated CNFs and TiO<sub>2</sub>@CNFs, respectively, after 120 min visible light irradiation. The reaction constants  $K_1$ ,  $K_2$ ,  $K_3$ , and  $K_4$  determined for initial dye concentration, reaction temperature, light intensity, and photocatalyst dose, respectively, are in full agreement with the estimated results from the model for the rate constant ( $k_{app}$ ). The results suggest further exploration of the electrospinning fabrication method for the synthesis and use of NiTiO<sub>3</sub>/TiO<sub>2</sub>-decorated CNFs towards effective photocatalytic activity and future applications in environmental remediation. The recyclability data of the synthesized NiTiO<sub>3</sub>/TiO<sub>2</sub>-decorated CNFs catalyst show that the catalyst is quite stable, and a very small decrease is observed in the MB photodegradation activity from 82.4 to 81.1% after 120 min of visible light irradiation for four consecutive runs. The data also showed good recyclability characteristics of the catalyst. The performance of our catalyst for MB photocatalytic degradation is compared with those reported in the literature and the NiTiO<sub>3</sub>/TiO<sub>2</sub>-decorated CNFs exhibit higher rate constant compared to other catalysts.

**Author Contributions:** Methodology, M.A.A.; Investigation, I.M.M.; Data curation, I.M.M.; Writing—review & editing, M.A.A. All authors have read and agreed to the published version of the manuscript.

**Funding:** The research was funded by the Deputyship for Research and Innovation, Ministry of Education in Saudi Arabia for funding this research work through the project number ISP22-27.

**Institutional Review Board Statement:** Not applicable.

**Data Availability Statement:** The data presented in this study are available from the corresponding author upon reasonable request.

**Acknowledgments:** The authors extend their appreciation to the Deputyship for Research and Innovation, Ministry of Education in Saudi Arabia for funding this research work through the project number ISP22-27.

**Conflicts of Interest:** The authors declare no conflict of interest.

## References

1. Houas, A.; Lachheb, H.; Ksibi, M.; Elaloui, E.; Guillard, C.; Herrmann, J.M. Photocatalytic degradation pathway of methylene blue in water. *Appl. Catal. B Environ.* **2001**, *31*, 145–157. [[CrossRef](#)]
2. Ràfols, C.; Barceló, D. Determination of mono- and disulphonated azo dyes by liquid chromatography–atmospheric pressure ionization mass spectrometry. *J. Chromatogr. A* **1997**, *777*, 177–192. [[CrossRef](#)]
3. Han, F.; Kambala, V.S.R.; Srinivasan, M.; Rajarathnam, D.; Naidu, R. Tailored titanium dioxide photocatalysts for the degradation of organic dyes in wastewater treatment: A review. *Appl. Catal. A Gen.* **2009**, *359*, 25–40. [[CrossRef](#)]
4. Yahya, N.; Aziz, F.; Jamaludin, N.; Mutalib, M.A.; Ismail, A.; Salleh, W.W.; Jaafar, J.; Yusof, N.; Ludin, N.A. A review of integrated photocatalyst adsorbents for wastewater treatment. *J. Environ. Chem. Eng.* **2018**, *6*, 7411–7425. [[CrossRef](#)]
5. Alshameri, A.; Ibrahim, A.; Assabri, A.M.; Lei, X.; Wang, H.; Yan, C. The investigation into the ammonium removal performance of Yemeni natural zeolite: Modification, ion exchange mechanism, and thermodynamics. *Powder Technol.* **2014**, *258*, 20–31. [[CrossRef](#)]
6. Kang, M.; Chen, H.; Sato, Y.; Kamei, T.; Magara, Y. Rapid and economical indicator for evaluating arsenic removal with minimum aluminum residual during coagulation process. *Water Res.* **2003**, *37*, 4599–4604. [[CrossRef](#)]
7. Yagub, M.T.; Sen, T.K.; Afroze, S.; Ang, H.M. Dye and its removal from aqueous solution by adsorption: A review. *Adv. Colloid Interface Sci.* **2014**, *209*, 172–184. [[CrossRef](#)]
8. Beluci, N.; Mateus, G.; Miyashiro, C.S.; Homem, N.; Gomes, R.G.; Fagundes-Klen, M.R.; Bergamasco, R.; Vieira, A.M.S. Hybrid treatment of coagulation/flocculation process followed by ultrafiltration in TiO<sub>2</sub>-modified membranes to improve the removal of reactive black 5 dye. *Sci. Total Environ.* **2019**, *664*, 222–229. [[CrossRef](#)]
9. Wu, J.; Eiteman, M.A.; Law, S.E. Evaluation of Membrane Filtration and Ozonation Processes for Treatment of Reactive-Dye Wastewater. *J. Environ. Eng.* **1998**, *124*, 272–277. [[CrossRef](#)]
10. Miranda-García, N.; Maldonado, M.I.; Coronado, J.; Malato, S. Degradation study of 15 emerging contaminants at low concentration by immobilized TiO<sub>2</sub> in a pilot plant. *Catal. Today* **2010**, *151*, 107–113. [[CrossRef](#)]
11. Nasir, A.M.; Jaafar, J.; Aziz, F.; Yusof, N.; Salleh, W.N.W.; Ismail, A.F.; Aziz, M. A review on floating nanocomposite photocatalyst: Fabrication and applications for wastewater treatment. *J. Water Process. Eng.* **2020**, *36*, 101300. [[CrossRef](#)]
12. Sathyajothi, S.; Jayavel, R.; Dhanemozhi, A.C. The Fabrication of Natural Dye Sensitized Solar Cell (Dssc) based on TiO<sub>2</sub> Using Henna and Beetroot Dye Extracts. *Mater. Today Proc.* **2017**, *4*, 668–676. [[CrossRef](#)]
13. Liu, Y.; Chen, X.; Li, J.; Burda, C. Photocatalytic degradation of azo dyes by nitrogen-doped TiO<sub>2</sub> nanocatalysts. *Chemosphere* **2005**, *61*, 11–18. [[CrossRef](#)] [[PubMed](#)]
14. Liang, Y.; Sun, S.; Deng, T.; Ding, H.; Chen, W.; Chen, Y. The Preparation of TiO<sub>2</sub> Film by the Sol-Gel Method and Evaluation of Its Self-Cleaning Property. *Materials* **2018**, *11*, 450. [[CrossRef](#)]
15. Reddy, K.R.; Hassan, M.; Gomes, V.G. Hybrid nanostructures based on titanium dioxide for enhanced photocatalysis. *Appl. Catal. A Gen.* **2015**, *489*, 838886. [[CrossRef](#)]
16. Nakhawong, R. Fabrication and characterization of MnTiO<sub>3</sub> nanofibers by sol–gel assisted electrospinning. *Mater. Lett.* **2015**, *161*, 468–470. [[CrossRef](#)]
17. Yamashita, H.; Harada, M.; Misaka, J.; Takeuchi, M.; Ikeue, K.; Anpo, M. Degradation of propanol diluted in water under visible light irradiation using metal ion-implanted titanium dioxide photocatalysts. *J. Photochem. Photobiol. A Chem.* **2002**, *148*, 257–261. [[CrossRef](#)]
18. In, S.; Orlov, A.; Berg, R.; García, F.; Pedrosa-Jimenez, S.; Tikhov, M.S.; Wright, D.S.; Lambert, R.M. Effective Visible Light-Activated B-Doped and B,N-Codoped TiO<sub>2</sub> Photocatalysts. *J. Am. Chem. Soc.* **2007**, *129*, 13790–13791. [[CrossRef](#)]
19. Ng, J.; Xu, S.; Zhang, X.; Yang, H.Y.; Sun, D.D. Hybridized Nanowires and Cubes: A Novel Architecture of a Heterojunctioned TiO<sub>2</sub>/SrTiO<sub>3</sub> Thin Film for Efficient Water Splitting. *Adv. Funct. Mater.* **2010**, *20*, 4287–4294. [[CrossRef](#)]
20. Han, T.; Chen, Y.; Tian, G.; Wang, J.-Q.; Ren, Z.; Zhou, W.; Fu, H. Hierarchical FeTiO<sub>3</sub>–TiO<sub>2</sub> hollow spheres for efficient simulated sunlight-driven water oxidation. *Nanoscale* **2015**, *7*, 15924–15934. [[CrossRef](#)]
21. Fang, D.; Huang, K.; Liu, S.; Luo, Z.; Qing, X.; Zhang, Q. High-density NiTiO<sub>3</sub>/TiO<sub>2</sub> nanotubes synthesized through sol–gel method using well-ordered TiO<sub>2</sub> membranes as template. *J. Alloys Compd.* **2010**, *498*, 37–41. [[CrossRef](#)]
22. Yang, W.; Yu, Y.; Starr, M.B.; Yin, X.; Li, Z.; Kvit, A.; Wang, S.; Zhao, P.; Wang, X. Ferroelectric Polarization-Enhanced Photoelectrochemical Water Splitting in TiO<sub>2</sub>–BaTiO<sub>3</sub> Core–Shell Nanowire Photoanodes. *Nano Lett.* **2015**, *15*, 7574–7580. [[CrossRef](#)] [[PubMed](#)]
23. Li, S.; Hu, S.; Jiang, W.; Liu, Y.; Zhou, Y.; Liu, Y.; Mo, L. Hierarchical architectures of bismuth molybdate nanosheets onto nickel titanate nanofibers: Facile synthesis and efficient photocatalytic removal of tetracycline hydrochloride. *J. Colloid Interface Sci.* **2018**, *521*, 42–49. [[CrossRef](#)] [[PubMed](#)]
24. Huang, J.; Jiang, Y.; Li, G.; Xue, C.; Guo, W. Hetero-structural NiTiO<sub>3</sub>/TiO<sub>2</sub> nanotubes for efficient photocatalytic hydrogen generation. *Renew. Energy* **2017**, *111*, 410–415. [[CrossRef](#)]
25. Huang, D.; Miyamoto, Y.; Ding, J.; Gu, J.; Zhu, S.; Liu, Q.; Fan, T.; Guo, Q.; Zhang, D. A new method to prepare high-surface-area N–TiO<sub>2</sub>/activated carbon. *Mater. Lett.* **2011**, *65*, 326–328. [[CrossRef](#)]
26. Muthirulan, P.; Meenakshisundaram, M.; Kannan, N. Beneficial role of ZnO photocatalyst supported with porous activated carbon for the mineralization of alizarin cyanin green dye in aqueous solution. *J. Adv. Res.* **2013**, *4*, 479–484. [[CrossRef](#)] [[PubMed](#)]

27. Wang, C.; Ao, Y.; Wang, P.; Hou, J.; Qian, J. Preparation, characterization and photocatalytic activity of a novel composite photocatalyst: Ceria-coated activated carbon. *J. Hazard. Mater.* **2010**, *184*, 1–5. [[CrossRef](#)]
28. Yousef, A.; Brooks, R.; Abutaleb, A.; El-Newehy, M.H.; Al-Deyab, S.S.; Kim, H.Y. One-step synthesis of Co-TiC-carbon composite nanofibers at low temperature. *Ceram. Int.* **2017**, *43*, 5828–5831. [[CrossRef](#)]
29. Yousef, A.; Brooks, R.M.; El-Halwany, M.; Abutaleb, A.; El-Newehy, M.H.; Al-Deyab, S.S.; Kim, H.Y. Electrospun CoCr<sub>7</sub>C<sub>3</sub>-supported C nanofibers: Effective, durable, and chemically stable catalyst for H<sub>2</sub> gas generation from ammonia borane. *Mol. Catal.* **2017**, *434*, 32–38. [[CrossRef](#)]
30. Moradi, M.; Vasseghian, Y.; Khataee, A.; Harati, M.; Arfaeinia, H. Ultrasound-assisted synthesis of FeTiO<sub>3</sub>/GO nanocomposite for photocatalytic degradation of phenol under visible light irradiation. *Sep. Purif. Technol.* **2021**, *261*, 118274. [[CrossRef](#)]
31. Yousef, A.; El-Halwany, M.M.; El-Newehy, M.H.; Al-Deyab, S.S.; Barakat, N.A.M. Synthesis of Cu–S-Codoped TiO<sub>2</sub> Nanoparticles Supported on Carbon Nanofibers for Simultaneous Adsorption and Photocatalytic Decomposition of Reactive Black 5. *J. Nanosci. Nanotechnol.* **2017**, *17*, 3998–4004. [[CrossRef](#)]
32. Unalan, H.E.; Wei, D.; Suzuki, K.; Dalal, S.; Hiralal, P.; Matsumoto, H.; Imaizumi, S.; Minagawa, M.; Tanioka, A.; Flewitt, A.J.; et al. Photoelectrochemical cell using dye sensitized zinc oxide nanowires grown on carbon fibers. *Appl. Phys. Lett.* **2008**, *93*, 133116. [[CrossRef](#)]
33. Liu, J.; Li, J.; Sedhain, A.; Lin, J.; Jiang, H. Structure and Photoluminescence Study of TiO<sub>2</sub> Nanoneedle Texture along Vertically Aligned Carbon Nanofiber Arrays. *J. Phys. Chem. C* **2008**, *112*, 17127–17132. [[CrossRef](#)]
34. Panthi, G.; Barakat, N.A.; Khalil, K.A.; Yousef, A.; Jeon, K.-S.; Kim, H.Y. Encapsulation of CoS nanoparticles in PAN electrospun nanofibers: Effective and reusable catalyst for ammonia borane hydrolysis and dyes photodegradation. *Ceram. Int.* **2013**, *39*, 1469–1476. [[CrossRef](#)]
35. Yousef, A.; Barakat, N.A.; Amna, T.; Al-Deyab, S.S.; Hassan, M.S.; Abdel-Hay, A.; Kim, H.Y. Inactivation of pathogenic *Klebsiella pneumoniae* by CuO/TiO<sub>2</sub> nanofibers: A multifunctional nanomaterial via one-step electrospinning. *Ceram. Int.* **2012**, *38*, 4525–4532. [[CrossRef](#)]
36. Yousef, A.; Barakat, N.A.; Kim, H.Y. Electrospun Cu-doped titania nanofibers for photocatalytic hydrolysis of ammonia borane. *Appl. Catal. A Gen.* **2013**, *467*, 98–106. [[CrossRef](#)]
37. Yousef, A.; Brooks, R.M.; El-Halwany, M.; El-Newehy, M.H.; Al-Deyab, S.S.; Barakat, N.A. Cu<sub>0</sub>/S-doped TiO<sub>2</sub> nanoparticles-decorated carbon nanofibers as novel and efficient photocatalyst for hydrogen generation from ammonia borane. *Ceram. Int.* **2016**, *42*, 1507–1512. [[CrossRef](#)]
38. Yousef, A.; Brooks, R.M.; El-Halwany, M.; Obaid, M.; El-Newehy, M.H.; Al-Deyab, S.S.; Barakat, N.A. A novel and chemical stable Co–B nanoflakes-like structure supported over titanium dioxide nanofibers used as catalyst for hydrogen generation from ammonia borane complex. *Int. J. Hydrogen Energy* **2016**, *41*, 285–293. [[CrossRef](#)]
39. Yousef, A.; El-Halwany, M.; Barakat, N.A.; Al-Maghrabi, M.N.; Kim, H.Y. Cu<sub>0</sub>-doped TiO<sub>2</sub> nanofibers as potential photocatalyst and antimicrobial agent. *J. Ind. Eng. Chem.* **2015**, *26*, 251–258. [[CrossRef](#)]
40. Ali, I.; Park, S.; Kim, J.-O. Modeling the photocatalytic reactions of g-C<sub>3</sub>N<sub>4</sub>-TiO<sub>2</sub> nanocomposites in a recirculating semi-batch reactor. *J. Alloys Compd.* **2020**, *821*, 153498. [[CrossRef](#)]
41. Wang, R.-C.; Yu, C.-W. Phenol degradation under visible light irradiation in the continuous system of photocatalysis and sonolysis. *Ultrason. Sonochem.* **2013**, *20*, 553–564. [[CrossRef](#)] [[PubMed](#)]
42. Alkaykh, S.; Mbarek, A.; Ali-Shattil, E.E. Photocatalytic degradation of methylene blue dye in aqueous solution by MnTiO<sub>3</sub> nanoparticles under sunlight irradiation. *Heliyon* **2020**, *6*, e03663. [[CrossRef](#)] [[PubMed](#)]
43. Mengyue, Z.; Shifu, C.; Yaowu, T. Photocatalytic degradation of organophosphorus pesticides using thin films of TiO<sub>2</sub>. *J. Chem. Technol. Biotechnol.* **1995**, *64*, 339–344. [[CrossRef](#)]
44. Ku, Y.; Chiu, P.-C.; Chou, Y.-C. Decomposition of aniline in aqueous solution by UV/TiO<sub>2</sub> process with applying bias potential. *J. Hazard. Mater.* **2010**, *183*, 16–21. [[CrossRef](#)] [[PubMed](#)]
45. Chen, Y.-W.; Hsu, Y.-H. Effects of Reaction Temperature on the Photocatalytic Activity of TiO<sub>2</sub> with Pd and Cu Cocatalysts. *Catalysts* **2021**, *11*, 966. [[CrossRef](#)]
46. Meng, Y.; Xia, S.; Pan, G.; Xue, J.; Jiang, J.; Ni, Z. Preparation and photocatalytic activity of composite metal oxides derived from Salen-Cu(II) intercalated layered double hydroxides. *Korean J. Chem. Eng.* **2017**, *34*, 2331–2341. [[CrossRef](#)]
47. Ojstršek, A.; Kleinschek, K.S.; Fakin, D. Characterization of nano-sized TiO<sub>2</sub> suspensions for functional modification of polyester fabric. *Surf. Coat. Technol.* **2013**, *226*, 68–74. [[CrossRef](#)]
48. Kumar, G.P.A. A Review on the Factors Affecting the Photocatalytic Degradation of Hazardous Materials. *Mater. Sci. Eng. Int. J.* **2017**, *1*, 106–114. [[CrossRef](#)]
49. Salimi, A.; Roosta, A. Experimental solubility and thermodynamic aspects of methylene blue in different solvents. *Thermochim. Acta* **2019**, *675*, 134–139. [[CrossRef](#)]
50. Ahmed, S.; Rasul, M.G.; Martens, W.N.; Brown, R.; Hashib, M.A. Heterogeneous photocatalytic degradation of phenols in wastewater: A review on current status and developments. *Desalination* **2010**, *261*, 3–18. [[CrossRef](#)]
51. Puma, G.L.; Yue, P.L. Effect of the Radiation Wavelength on the Rate of Photocatalytic Oxidation of Organic Pollutants. *Ind. Eng. Chem. Res.* **2002**, *41*, 5594–5600. [[CrossRef](#)]
52. Kaneco, S.; Rahman, M.A.; Suzuki, T.; Katsumata, H.; Ohta, K. Optimization of solar photocatalytic degradation conditions of bisphenol A in water using titanium dioxide. *J. Photochem. Photobiol. A Chem.* **2004**, *163*, 419–424. [[CrossRef](#)]

53. Giannakoudakis, D.A.; Farahmand, N.; Łomot, D.; Sobczak, K.; Bandosz, T.J.; Colmenares, J.C. Ultrasound-activated TiO<sub>2</sub>/GO-based bifunctional photoreactive adsorbents for detoxification of chemical warfare agent surrogate vapors. *Chem. Eng. J.* **2020**, *395*, 125099. [[CrossRef](#)]
54. Fathinia, M.; Khataee, A. Photocatalytic ozonation of phenazopyridine using TiO<sub>2</sub> nanoparticles coated on ceramic plates: Mechanistic studies, degradation intermediates and ecotoxicological assessments. *Appl. Catal. A Gen.* **2015**, *491*, 136–154. [[CrossRef](#)]
55. Soltani, R.D.C.; Rezaee, A.; Khataee, A.; Safari, M. Photocatalytic process by immobilized carbon black/ZnO nanocomposite for dye removal from aqueous medium: Optimization by response surface methodology. *J. Ind. Eng. Chem.* **2014**, *20*, 1861–1868. [[CrossRef](#)]
56. Daneshvar, N.; Rabbani, M.; Modirshahla, N.; Behnajady, M. Kinetic modeling of photocatalytic degradation of Acid Red 27 in UV/TiO<sub>2</sub> process. *J. Photochem. Photobiol. A Chem.* **2004**, *168*, 39–45. [[CrossRef](#)]
57. Kim, Y.J.; Gao, B.; Han, S.Y.; Jung, M.H.; Chakraborty, A.K.; Ko, T.; Lee, C.; Lee, W.I. Heterojunction of FeTiO<sub>3</sub> Nanodisc and TiO<sub>2</sub> Nanoparticle for a Novel Visible Light Photocatalyst. *J. Phys. Chem. C* **2009**, *113*, 19179–19184. [[CrossRef](#)]
58. Yang, B.; Bai, X.; Wang, J.; Fang, M.; Wu, X.; Liu, Y.; Huang, Z.; Lao, C.-Y.; Min, X. Photocatalytic Performance of NiO/NiTiO<sub>3</sub> Composite Nanofiber Films. *Catalysts* **2019**, *9*, 561. [[CrossRef](#)]
59. Gao, B.; Kim, Y.J.; Chakraborty, A.K.; Lee, W.I. Efficient decomposition of organic compounds with FeTiO<sub>3</sub>/TiO<sub>2</sub> heterojunction under visible light irradiation. *Appl. Catal. B Environ.* **2008**, *83*, 202–207. [[CrossRef](#)]
60. Zhang, M.; Shao, C.; Mu, J.; Huang, X.; Zhang, Z.; Guo, Z.; Zhang, P.; Liu, Y. Hierarchical heterostructures of Bi<sub>2</sub>MoO<sub>6</sub> on carbon nanofibers: Controllable solvothermal fabrication and enhanced visible photocatalytic properties. *J. Mater. Chem.* **2012**, *22*, 577–584. [[CrossRef](#)]
61. Sivakumar, S.; Selvaraj, A.; Ramasamy, A.K. Photocatalytic Degradation of Organic Reactive Dyes over MnTiO<sub>3</sub>/TiO<sub>2</sub> Heterojunction Composites Under UV-Visible Irradiation. *Photochem. Photobiol.* **2013**, *89*, 1047–1056. [[CrossRef](#)] [[PubMed](#)]
62. Marco Alejandro Ruiz, P. Synthesis, Characterization and Photocatalytic Response of NiTiO<sub>3</sub>-Based Semiconducting Oxides. Ph.D. Thesis, Université du Maine, Le Mans, France, 2016.
63. Dao, D.Q.; Nguyen, T.K.A.; Pham, T.-T.; Shin, E.W. Synergistic Effect on Photocatalytic Activity of Co-Doped NiTiO<sub>3</sub>/g-C<sub>3</sub>N<sub>4</sub> Composites under Visible Light Irradiation. *Catalysts* **2020**, *10*, 1332. [[CrossRef](#)]
64. Kitchamsetti, N.; Didwal, P.N.; Mulani, S.R.; Patil, M.S.; Devan, R.S. Photocatalytic activity of MnTiO<sub>3</sub> perovskite nanodiscs for the removal of organic pollutants. *Heliyon* **2021**, *7*, e07297. [[CrossRef](#)] [[PubMed](#)]
65. Sadjadi, M.; Mozaffari, M.; Enhessari, M.; Zare, K. Effects of NiTiO<sub>3</sub> nanoparticles supported by mesoporous MCM-41 on photoreduction of methylene blue under UV and visible light irradiation. *Superlattices Microstruct.* **2010**, *47*, 685–694. [[CrossRef](#)]
66. Khan, H.; Kang, S.; Lee, C. Evaluation of Efficient and Noble-Metal-Free NiTiO<sub>3</sub> Nanofibers Sensitized with Porous gC<sub>3</sub>N<sub>4</sub> Sheets for Photocatalytic Applications. *Catalysts* **2021**, *11*, 385. [[CrossRef](#)]

**Disclaimer/Publisher's Note:** The statements, opinions and data contained in all publications are solely those of the individual author(s) and contributor(s) and not of MDPI and/or the editor(s). MDPI and/or the editor(s) disclaim responsibility for any injury to people or property resulting from any ideas, methods, instructions or products referred to in the content.